Metallophysics and Advanced Technologies
Металофіз. новітні технол.
Metallofiz. Noveishie Tekhnol.
2024, vol. 46, No. 6, pp. 517–529
https://doi.org/10.15407/mfint.46.06.0517
Reprints available directly from the publisher

PACS numbers: 73.63.Rt, 74.25.Gz, 74.78.-w, 74.81.-g, 75.47.Lx, 84.37.+q, 85.25.Am

Inhomogeneous Resistivity of Transparent Superconductor Films Revealed by the Van Der Pauw Technique

A. Shapovalov[*], D. Menesenko[*,**], E. Zhitlukhina[***,****], A. Parra[*****], A. Aliev[*****], V. Shamaev[******], M. Gregor[****], and T. Plecenik[****]

[*]*Kyiv Academic University, N.A.S. of Ukraine and M.E.S. of Ukraine, 36 Academician Vernadsky Blvd., UA-03142 Kyiv, Ukraine*
[**]*G. V. Kurdyumov Institute for Metal Physics, N.A.S. of Ukraine, 36 Academician Vernadsky Blvd., UA-03142 Kyiv, Ukraine*
[***]*Donetsk Institute for Physics and Engineering Named after O. O. Galkin, N.A.S. of Ukraine, 46 Nauky Ave., UA-03028 Kyiv, Ukraine*
[****]*Centre for Nanotechnology and Advanced Materials, Faculty of Mathematics, Physics and Informatics, Comenius University Bratislava, F2 Mlynská dolina, 84248 Bratislava, Slovak Republic*
[*****]*Alan G. MacDiarmid NanoTech Institute, University of Texas at Dallas, 800 West Campbell Road., TX-75080 Richardson, USA*
[******]*Donetsk National Technical University, 2 Shybankov Sqr., UA-85300 Pokrovs'k, Ukraine*

Detection of structural and transport inhomogeneities in superconducting thin films using the standard four-probe method requires multiple measurements and may be inaccurate. A new approach to extract the information about the inhomogeneous transition into the superconducting state using van der Pauw technique is presented. The proposed method is applied to an elec-

Corresponding author: Andriy Petrovych Shapovalov
E-mail: shapovalovap@gmail.com

Citation: A. Shapovalov, D. Menesenko, E. Zhitlukhina, A. Parra, A. Aliev, V. Shamaev, M. Gregor, and T. Plecenik, Inhomogeneous Resistivity of Transparent Superconductor Films Revealed by the Van Der Pauw Technique, *Metallofiz. Noveishie Tekhnol.*, **46**, No. 6: 517–529 (2024). DOI: 10.15407/mfint.46.06.0517

trochemically-reduced In–Sn-oxide (ITO) films known to be simultaneously transparent and superconducting. Relationship between the processing parameters and superconducting characteristics of the ITO films is considered, and prospects for using such samples in integrated photonic-superconducting chips for quantum-information processing are discussed.

Key words: transparent superconductivity, doped In–Sn oxide, four-point resistance, temperature and angular dependences.

Виявлення структурної та транспортної неоднорідностей у надпровідних тонких плівках за допомогою стандартного чотироточкового методу вимагає багаторазових мірянь і може бути неточним. Представлено новий підхід щодо одержання інформації про неоднорідний перехід у надпровідний стан за допомогою методики ван-дер-Пау. Запропонований метод застосовано до електрохемічно відновлених плівок оксиду Індію й Стануму (ICO), які є водночас прозорими та надпровідними. Розглянуто зв'язок між параметрами оброблення та надпровідними характеристиками плівок ICO й обговорено перспективи використання таких зразків в інтеґрованих фотон-надпровідних чіпах для квантового оброблення інформації.

Ключові слова: прозора надпровідність, леґований In–Sn-оксид, чотироточковий опір, температурна та кутова залежності.

(Received 8 April, 2024; in final version, 6 May, 2024)

1. INTRODUCTION

The most popular technique for finding resistivity of a homogeneous material is the four-probe method. When the resistance R of a rectangular sample with a cross sectional area A and voltage probe separation l is measured, the resistivity ρ can be easily calculated as $\rho = RA/l$. In heterogeneous films, the standard four-point procedure requires many measurements and may be hence imprecise due to the difficulty of accurately measuring the geometric A/l factor [1]. In non-uniform materials, an additional source of error arises from insufficient number of measurements. Because of this, new methods using planar samples were proposed. One such approach developed by van der Pauw (vdP) [2, 3] can be applied to films of arbitrary shape and uses four point contacts on the sample periphery. The most important issue of this technique is that measurements using the vdP method give a weighted average of local resistances of the sample, whereas the traditional linear layout of the four contacts provides knowledge of resistivity only in the probing direction [4].

In the vdP configuration, a current is flowing along one edge of the sample (for instance, I_{12}) while the voltage bias is applied across the opposite edge (in this case, V_{34}). The ratio of the potential drop V_{34} and the current I_{12} has units of resistance and is known as the 'four-probe

resistance' $R_{12,34} = V_{34}/I_{12}$ [4, 5]. According to the reciprocity theorem, when the current I in one branch of a reciprocal network composing of linear elements produces a voltage drop V in opposite side, the insertion of I into the opposite side must give the same voltage drop V in the first branch: $R_{12,34} = R_{34,12}$ [4]. It is clear that this statement is valid only for electrical circuits without non-reciprocal (*e.g.*, a rectifying diode) and/or nonlinear elements destroying reciprocity.

Therefore, in a network of ordinary impedances, additional information within a four-probe method can be obtained only by rotating the contact system to 90 degrees while current flows between 2 and 3 points and voltage is applied to 4 and 1 contacts. In this case, $R_{23,41} = V_{41}/I_{23}$. Solving the general problem of potential distribution in thin conductive layers, van der Pauw showed that the sheet resistance R of samples with arbitrary shapes can be found from the relation:

$$\exp(-\pi R_{12,34} / R) + \exp(-\pi R_{23,41} / R) = 1 . \quad (1)$$

In general, the van der Pauw's formula (1) cannot be reformulated to determine R in terms of conventional functions. The most important exception to this statement is when $R_{23,41} = R_{12,34} = R^*$; then, the sheet resistance is given by the simple expression:

$$R = \pi R^* / \ln 2 = 4.53 R^* . \quad (2)$$

Although the vdP method seems relatively simple and universal, it has a number of important limitations. The thickness d of the studied film, which should not have holes and/or islands of highly conductive material, has to be uniform and small in relation to the distance between the probes. Besides, the samples must be homogeneous and isotropic. The authors of the work [4] drew attention to the fact that the vdP technique can lead to non-physical results in rather inhomogeneous samples and, to confirm this, proposed a simplified four-resistor model that was applied in Ref. [4] to a square sample. Following the model, where a square thin layer is conditionally divided into four resistive regions, we propose an equivalent circuit with a current source and four resistors R_i ($i = 1, 2, 3, 4$) for the analysis of resistance measurements in superconducting films (see below Fig. 1).

This study focuses on expanding vdP measurements to superconducting layers at temperatures near the critical temperature T_c, when the resistance of the sample abruptly drops from a finite value to zero. In this regard, local inhomogeneities of the superconducting films, namely, spatial variations in T_c and the widths of the resistance drop ΔT_c are directly reflected in the measured four-probe characteristics [6, 7]. The main focus is on the thin layers of indium–tin oxide (ITO), a degenerate semiconductor material with wide band gap and high con-

ductivity that is obtained by doping high-mobility semiconductor In_2O_3 with a small amount of Sn [8]. The most important property for our work is the ability of ITO to exhibit superconductivity under specific processing conditions [9–11]. Below, we present our method to analyse the inhomogeneity of the superconducting order parameter that is applied to $In_{2-y}Sn_yO_{3-\delta}$ ($y \cong 0.2$) thin films electrochemically reduced in an aqueous solution by sodium or magnesium ions. Our main concern is about the relationship between processing parameters and superconducting characteristics of the ITO films and prospects for using such samples in integrated photonic-superconducting chips for quantum information processing [12].

2. MODELLING

The simplified four-resistor model for analysing the vdP measurement data is shown in Fig. 1 for two configurations A and B used in the vdP formalism and discussed above. Below, we use these two contact arrangements in order to analyse near-T_c resistance *vs.* temperature data for superconducting ITO films. Let us start with the A case. Using first and second Kirchhoff laws, we obtain the following relationships for currents in the circuit (see Fig. 1): $I = I'' + I'$ and $I''(R_{23} + R_{34} + R_{41}) - I''R_{12} = 0$. Their combination gives us the following result: $I'(R_{12} + R_{23} + R_{34} + R_{41}) = IR_{12}$; hence, $I = I'(R_{12} + R_{23} + R_{34} + R_{41})/R_{12}$. The ratio of the potential drop $V = I'R_{34}$ across the resistor R_{34} and the applied current I is the 'four-probe resistance' $R^{(A)} = V/I$ [4,

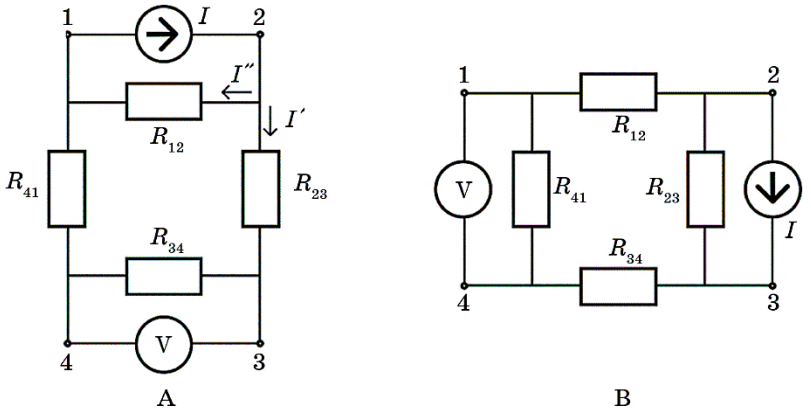

Fig. 1. Four-resistor equivalent circuits (A and B configurations) for vdP resistive measurements of a square superconducting layer conditionally divided into four resistive regions. The analysed resistance R(A) is the ratio of the voltage drop across R_{34} to the total applied current $I_{1,2}$ through the network, while R(B) is the ratio of the voltage drop across R_{41} to the applied current $I_{2,3}$.

5]. Thus, for the configurations A and B, we get:

$$R^{(\mathrm{A})} = \frac{R_{12}R_{34}}{R_{12}+R_{23}+R_{34}+R_{41}},\ R^{(\mathrm{B})} = \frac{R_{23}R_{41}}{R_{12}+R_{23}+R_{34}+R_{41}}. \qquad (3)$$

In contrast with previous works, we are dealing with a comparatively sharp variation of the resistances which will be approximated by identical formulas $R(T) = R^*(1 + \mathrm{th}((T - T_c)/\Delta T_c))$, where R^* is identified with a middle point of the resistive transition usually determined as a value between 10 and 90% resistivity drop. In the case of superconducting granularity, different resistors in the equivalent circuit picture are representing different sectors of the layer which may have slightly different transition temperatures T_c and the transition widths ΔT although in the normal state, the samples are homogeneous. Figures 2 and 3 demonstrate how the shape of $R^{(\mathrm{A})}(T)$ and $R^{(\mathrm{B})}(T)$ curves can be radically distorted with relatively small local changes in T_c and ΔT_c values.

In particular, it relates a near-T_c resistive peak in R *vs.* T curves sometimes associated with such physical effects as the mismatch between quasiparticle and cooper pair potentials [13], phase-slip events [14], an interaction between superconducting fluctuations and conduction electrons [15], proximity-caused effects at the superconductor/ferromagnetic interface [16]. Figure 3 shows resistance characteristics imitating re-entrant superconductivity phenomenon [17]. There-

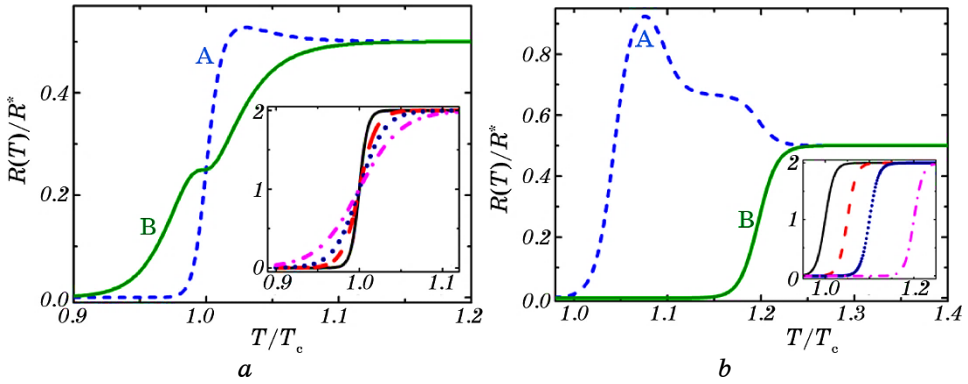

Fig. 2. Calculated resistance-*versus*-temperature characteristics for two different scenarios A and B, $R_A(T)$ (dashed curve) and $R_B(T)$ (solid curve), respectively: superconducting transition widths in the film sections $\Delta T_{c12} = 0.01T_c$, $\Delta T_{c23} = 0.03T_c$, $\Delta T_{c34} = 0.02T_c$, $\Delta T_{c41} = 0.05T_c$, while T_c is the same: $T_{c12} = T_{c23} = T_{c34} = T_{c41} = T_c$ (*a*), and the critical temperature in the film sections differs from each other $T_{c12} = T_c$, $T_{c23} = 1.1T_c$, $T_{c34} = 1.05T_c$, $T_{c41} = 1.2T_c$, while ΔT_c is the same $\Delta T_{c12} = \Delta T_{c23} = \Delta T_{c34} = \Delta T_{c41} = 0.02T_c$ (*b*). The insets show $R(T)$ curves for the sections 12, 23, 34, and 41 (solid, dashed, dotted, and dashed-dotted curves, respectively).

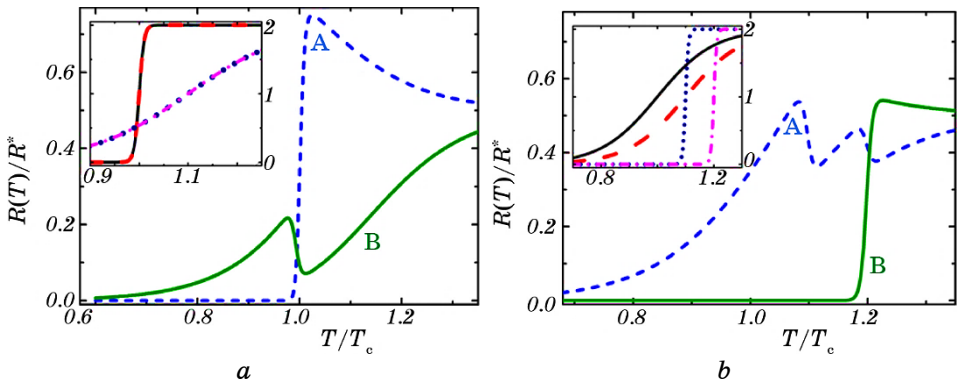

Fig. 3. Calculated resistance-versus-temperature characteristics for two different scenarios A and B, $R_A(T)$ (dashed curve) and $R_B(T)$ (solid curve), respectively: superconducting transition widths in the film sections $\Delta T_{c12} = \Delta T_{c34} = 0.01 T_c$, $\Delta T_{c23} = \Delta T_{c41} = 0.2 T_c$, while T_c is $T_{c12} = T_{c34} = T_c$, $T_{c23} = T_{c41} = 1.1 T_c$ (*a*), and the critical temperatures in the film sections differ from those in the others $T_{c12} = T_c$, $T_{c23} = T_{c34} = 1.1 T_c$, $T_{c41} = 1.2 T_c$, while $\Delta T_{c12} = \Delta T_{c34} = 0.2 T_c$, $\Delta T_{c23} = \Delta T_{c41} = 0.01 T_c$ (*b*). The insets show $R(T)$ curves for the sections 12, 23, 34, and 41 (solid, dashed, dotted, and dashed-dotted curves, respectively).

fore, as argued in our previous publications [6, 7], an unusual shape of the vdP resistance *vs.* temperature traces and strong difference between the characteristics for the two configurations A and B can serve as a qualitative indicator of the presence of superconducting granularity in the sample studied.

3. CHARACTERIZATION OF THE ITO FILMS

The electrochemical processing of thin films is a powerful method for tuning physical and chemical properties of the base material whose structural evolution is expected to be more striking than that of bulk counterparts making it easier to explore new physics in the quantum limit [18, 19]. It was previously shown that such treatment leads to an improvement of superconducting characteristics [10, 11]. In our case, this technique was applied to commercially available ITO layers with thickness of about 350 nm. The control of charge injection was performed by varying charging times at a fixed current of 0.1 mA/cm^2 in an aqueous solution of 2 mol NaCl or MgCl. Such treatment led to the enhancement of superconducting properties from the critical temperature T_c lower than 0.3 K for the parent compound to $T_c = 4$–5 K, at that the films acquire colour from transparent yellowish to dark brown, possibly by increasing the electron density.

X-ray spectra of our ITO films reduced with magnesium chloride show an increase in the presence of a reduced metal layer on the surface (Fig. 4). When the charge injection time is less than 1000 s, the transparency of the film allows visual monitoring of inhomogeneity using an optical microscope. Most often, the colouring turned out to be uneven.

The SEM results in Fig. 5 show that the surface structure of the investigated ITO films changes significantly with increasing reduction time. For a shorter time (Fig. 5, *a*), we see islands or clusters of two types, with a longitudinal grain boundary and with a rounded boundary, while all grains are more or less commensurate. In addition, there are dark areas that look very similar to holes. On the other hand, when the reduction is shortened by approximately 8000 seconds (Figs. 5, *b* and *c*), the image transforms into a more homogeneous medium with different sizes of grain boundaries and some regions where the grains do not seem to be connected to the sample area, as seen in Fig. 5, *c*.

Structural analysis based on the XRD data shows the appearance of indium metal peaks and the smoothing of ITO peaks depending on the increase in the time of electrochemical reduction of the samples. SEM images reveal strong surface structural variations observed by other authors using aqueous electrolytes as well [20]. Such changes are explained by composition deoxidation, which leads to the formation of metallic indium and tin phases in the material.

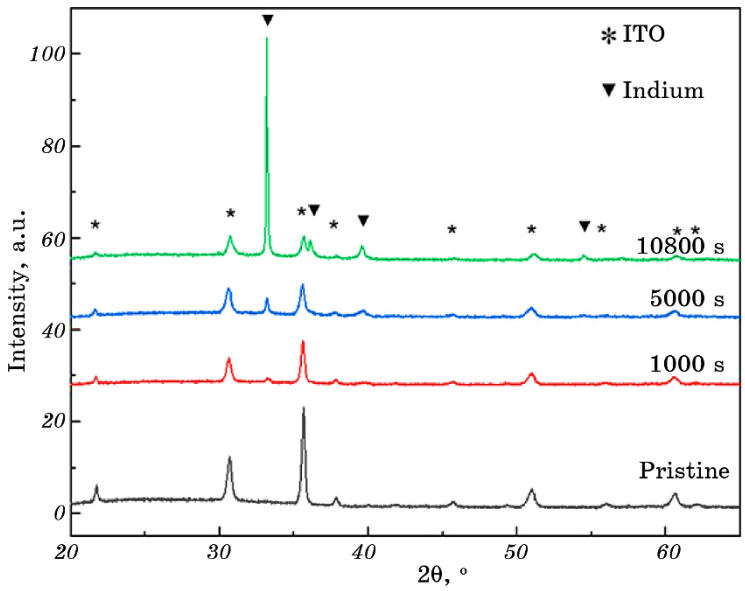

Fig. 4. XRD spectra of pristine ITO (G002), 1000 s, 5000 s and 10800 s, reduced ITO in 2 mol MgCl at a current density of 0.1 A/cm^2. Peaks associated with ITO and metallic indium are marked with asterisks and triangles, respectively.

4. RESISTIVE MEASUREMENTS AND DISCUSSION

Resistance *vs*. temperature characteristics of the ITO films $R_A(T)$ and $R_B(T)$ were measured using the physical property measurements system (PPMS, DynaCool, Quantum Design, Inc.) for the two combinations of current-carrying and voltage contacts shown in Fig. 1 in magnetic fields from zero to 1 T in 0.2 T increments and the orientations varied from zero (perpendicular to the layer) to 90° (parallel to the surface of the layer) in 30° increments. The measured curves were analysed using Eqs. (3) with temperature-dependent resistances.

Figures 6 and 7 show representative $R_A(T)$ and $R_B(T)$ traces normalized to the above-T_c resistance value R_{10} measured at 10 K for different reduction time. Figures 8 and 9 demonstrate an impact of the spatial orientation of a fixed magnetic field on representative $R_A(T)$ and $R_B(T)$ curves normalized to the resistance value R_{10} at 10 K for samples with relatively large reduction times.

The main conclusions following from the dependence of resistance on temperature and angular dependence are as follows. A near-T_c resistive peak in Fig. 6 indicates huge heterogeneity of superconducting properties of the films reduced in NaCl electrolyte at relatively short reduction times up to 500 s. At the same time, films reduced in MgCl (Fig. 7) exhibit rather uniform properties and, at reduction time of 750 s, the resistance *vs*. temperature curves are practically identical for two configurations A and B.

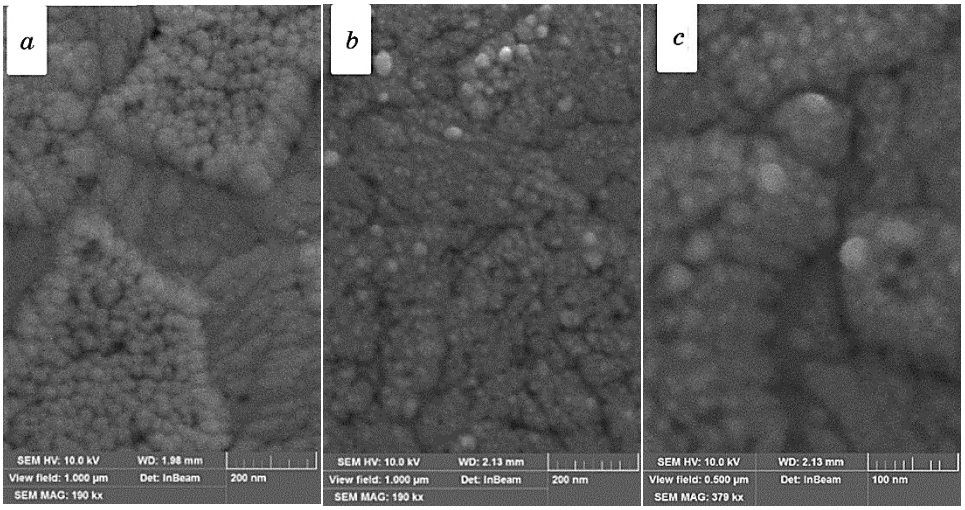

Fig. 5. SEM images of two reduced ITO superconducting films in the MgCl water electrolyte for reduction times of 500 seconds (*a*) and 8000 seconds (*b*, *c*).

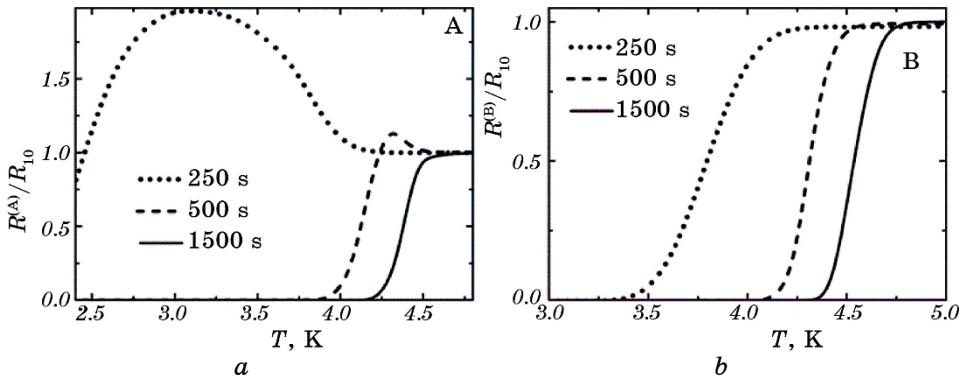

Fig. 6. Representative four-probe $R^{(A)}(T)$ and $R^{(B)}(T)$ curves normalized to the resistance value R_{10} at 10 K for two different contact arrangements (see Fig. 1) measured on three reduced in NaCl ITO superconducting films with increasing reduction times of 250, 500, and 1500 seconds.

The next issue is the dimensionality of the superconducting state in studied samples [7] and the effect of the surface scatterings on resistivity of thin films [21].

The angular dependencies of the film resistances (Figs. 8 and 9) show that the samples with the reduction times of 1000 s and more are conventional three-dimensional superconductors with a very small surface-derived effect, see the related discussion in our paper [7]. This result contradicts the assumption of the authors of the work [22] that the electrochemical reduction lead to the formation of a dense thin film of nanoparticles on top of the ITO layer which is the source of the dissipa-

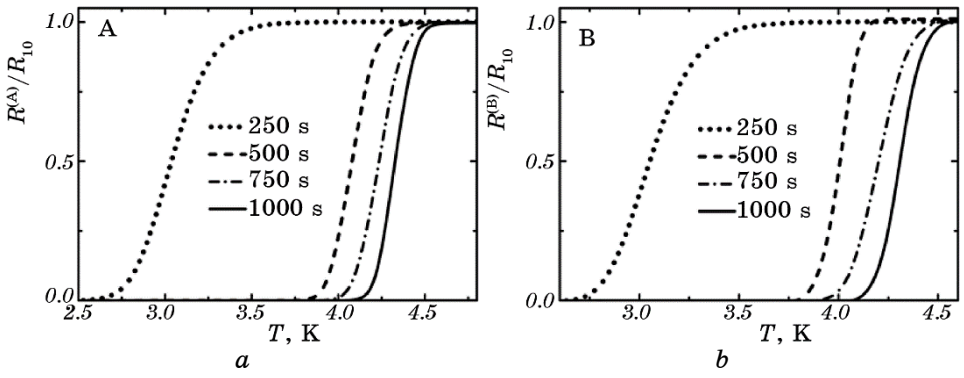

Fig. 7. Representative four-probe $R^{(A)}(T)$ and $R^{(B)}(T)$ curves normalized to the resistance value R_{10} at 10 K for two different contact arrangements (see Fig. 1) measured on four reduced in MgCl ITO superconducting films with increasing reduction times of 250, 500, 750 and 1000 seconds.

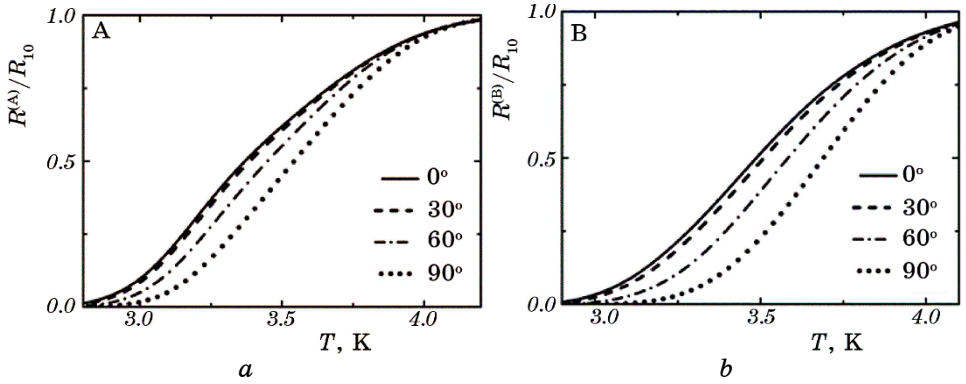

Fig. 8. Angular dependence of four-probe $R^{(A)}(T)$ and $R^{(B)}(T)$ characteristics for reduced in NaCl ITO superconducting film with a 1000 s reduction time in the field of 0.2 T for different contact arrangements (see Fig. 1). The angles are formed by the field with a normal to the film surface.

tionless superconducting state. The observed three-dimensional superconductivity also indicates that bulk structural changes are occurring.

Let us briefly discuss why ITO samples are transparent. The optical band gap measured using optical techniques determines the energy required for excitation of a single electron from the valence band maximum to the conduction band minimum. To ensure optical transparency, it should be larger than 3 eV that corresponds to the maximum wavelength of visible photons. For many materials, the onset of strong absorption occurs at the direct band gap, when the edge states of the two bands correspond to the same wave vector **k** in the reciprocal space.

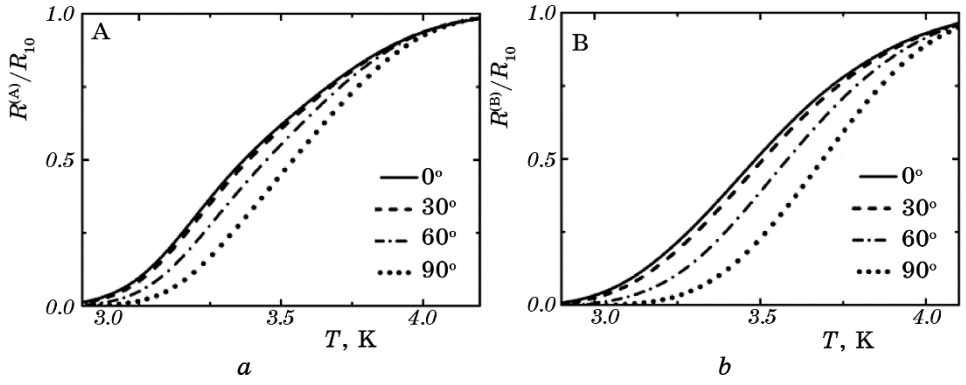

Fig. 9. Angular dependence of four-probe $R^{(A)}(T)$ and $R^{(B)}(T)$ characteristics for reduced in MgCl ITO superconducting film with a 1000 s reduction time in the field of 0.2 T for different contact arrangements (see Fig. 1). The angles are formed by the field with a normal to the film surface.

Then an incident photon with sufficient energy can cause an electron to transfer between the states with a momentum of the resulting electron–hole pair very close to zero. However, some direct transitions can be forbidden due to specific selection rules governing symmetry, parity, and spin such that the onset of the absorption edge occurs at higher energies than the direct gap. For example, it relates the *n*-type Sn-doped In_2O_3 (ITO) oxide with a fundamental direct band gap of 2.9 eV where the first strong transitions occur from valence bands 0.81 eV below the valence-band maximum [23]. In addition to the increase from the Burstein–Moss effect, it leads to the onset of strong optical absorption at 3.75 eV [23].

As was emphasized by Woods-Robinson *et al.* [24], the presence of forbidden optical transitions at gap edges can be an important factor in enhancing transparency. To address this, the authors computed absorption spectra across nearly 18.000 inorganic compounds in the Materials Project database, showing that over half of the selected semiconductors exhibit forbidden or weak absorption edges. From this set of materials, the authors suggested a list of candidates for *n*- or *p*-type transparent conducting materials with forbidden band edge transitions and promising optical and electronic characteristics. Their main methodological conclusion is that in the search for new materials that are both transparent and conductive, metrics representing absorption spectra, not just bandgap, should be used.

We believe that the ITO and similar films can form a basis of novel hybrid electronics integrating optical and superconducting components since the use of transparent superconducting materials provides a perfect solution to avoid significant losses due to photon absorption in such on-chip circuits. This also applies to data transmission in a quantum network formed by quantum computers based on superconducting qubits [25]. Important application is single-photon detectors for sensing based on the cooper-pair breaking effect. At last, integration of photonic components offering few-photon and light-speed communication with superconducting ones providing fast and energy-efficient computation in neuromorphic applications ensures synaptic time constants spanning four orders of magnitude from hundreds of nanoseconds to milliseconds [26].

5. SUMMARY

In the paper, we have used the van der Pauw contact placement and four-probe resistance measurements for two configurations in order to analyse near-T_c resistance *vs.* temperature data for transparent superconducting ITO films. As was shown in our previous publications [6, 7], unusual shape of such nonlocal four-probe resistance characteristics can serve as a qualitative indicator of the presence of superconducting

granularity in the sample studied. The angular variations in film resistivity indicate that the samples subjected to a reduction time of 1000 seconds or more exhibit characteristics similar to those of conventional three-dimensional superconductors with a minimal surface effect. At last, we hope that this technique applied to transparent conducting oxides will be useful for further progress of the transparent superconducting electronics, which is currently still in its very early stages.

The research of transparent superconductors is supported by the NATO Science for Peace and Security Program, project SPS G6082. This work was supported in part by the Slovak Research and Development Agency under contracts no. APVV-19-0365 and APVV-19-0303 as well as under the Operational Program Integrated Infrastructure for the projects Advancing University Capacity and Competence in Research, Development and Innovation (ACCORD, ITMS2014+: 313021X329) and UpScale of Comenius University Capacities and Competence in Research, Development and Innovation (USCCCORD, ITMS 2014+: 313021BUZ3), co-financed by the European Regional Development Fund. E.Zh. acknowledges the EU NextGenerationEU financial support through the Recovery and Resilience Plan for Slovakia under the project No. 09I03-03-V01-00140.

REFERENCES

1. H. Wang, W. Porter, H. Bottner, J. Konig, L. Chen, S. Bai, T. Tritt, A. Mayolet, J. Senawiratne, C. Smith, F. Harris, P. Gilbert, J. Sharp, J. Lo, H. Kleinke, and L. Kiss, *J. Electron. Mater.*, **42**: 654 (2013).
2. L. J. van der Pauw, *Philips Res. Rep.*, **13**: 1 (1958).
3. L. J. van der Pauw, *Philips Tech. Rev.*, **20**: 220 (1958).
4. D. W. Koon and C. J. Knickerbocker, *Rev. Sci. Instrum.*, **63**: 207 (1992).
5. S. B. Kjeldby, O. M. Evenstad, S. P. Cooil, and J. W. Wells, *J. Phys.: Condens. Matter*, **29**: 394008 (2017).
6. M. Poláčková, E. Zhitlukhina, M. Belogolovskii, M. Gregor, T. Plecenik, and P. Seidel, *Eur. Phys. J. Plus*, **138**: 486 (2023).
7. M. Belogolovskii, M. Poláčková, E. Zhitlukhina, B. Grančič, L. Satrapinskyy, M. Gregor, and T. Plecenik, *Sci. Rep.*, **13**: 19450 (2023).
8. H. Ohta, M. Orita, M. Hirano, H. Tanji, H. Kawazoe, and H. Hosono, *Appl. Phys. Lett.*, **76**: 2740 (2000).
9. N. Mori, *J. Appl. Phys.*, **73**: 1327 (1993).
10. A. E. Aliev, K. Xiong, K. Cho, and M. B. Salamon, *Appl. Phys. Lett.*, **101**: 252603 (2012).
11. A. E. Aliev, M. Jung de Andrade, and M. B. Salamon, *J. Supercond. Nov. Magn.*, **29**: 1793 (2016).
12. X.-B. Xu, W.-T. Wang, L.-Y. Sun, and C.-L. Zou, *Chip*, **1**: 100016 (2022).
13. Y. K. Kwong, K. Lin, P. J. Hakonen, M. S. Isaacson, and J. M. Parpia, *Phys. Rev. B*, **44**: 462 (1991).
14. E. Rudenko, D. Solomakha, I. Korotash, P. Febvre, E. Zhitlukhina, and

M. Belogolovskii, *IEEE Trans. Appl. Supercond.*, **27**: 1800105 (2016).
15. J. M. Gordon and A. M. Goldman, *Phys. Rev. B*, **34**: 1500 (1986).
16. A. K. Singh, U. Kar, M. D. Redell, T. C. Wu, W. H. Peng, B. Das, S. Kumar, W.-C. Lee, and W. L. Lee, *npj Quantum Mater.*, **5**: 45 (2020).
17. S. V. Postolova, A. Yu. Mironov, M. R. Baklanova, V. M. Vinokur, and T. I. Baturina, *Sci. Rep.*, **7**: 1718 (2017).
18. J. Wan, S. D. Lacey, J. Dai, W. Bao, M. S. Fuhrer, and L. Hu, *Chem. Soc. Rev.*, **45**: 6742 (2016).
19. M. S. Stark, K. L. Kuntz, S. J. Martens, and S. C. Warren, *Adv. Mater.*, **31**: 1808213 (2019).
20. L. Liu, S. Yellinek, I. Valdinger, A. Donval, and D. Mandler, *Electrochim. Acta*, **176**: 1374 (2015).
21. M. A. Belogolovskii, Y. F. Revenko, A. Y. Gerasimenko, V. M. Svistunov, E. Hatta, G. Plitnik, V. E. Shaternik, and E. M. Rudenko, *Low Temp. Phys.*, **28**: 391 (2002).
22. E. Batson, M. Colangelo, J. Simonaitis, E. Gebremeskel, O. Medeiros, M. Saravanapavanantham, V. Bulovic, P. D. Keathley, and K. K. Berggren, *Supercond. Sci. Technol.*, **36**: 055009 (2023).
23. A. Walsh, J. L. Da Silva, S.-H. Wei, C. Körber, A. Klein, L. Piper, A. DeMasi, K. E. Smith, G. Panaccione, P. Torelli, D. J. Payne, A. Bourlange, and R. G. Egdell, *Phys. Rev. Lett.*, **100**: 167402 (2008).
24. R. Woods-Robinson, Y. Xiong, J.-X. Shen, N. Winner, M. K. Horton, M. Asta, A. M. Ganose, G. Hautier, and K. A. Persson, *Matter*, **6**: 3021 (2023).
25. E. Zhitlukhina, M. Belogolovskii, and P. Seidel, *IEEE Trans. Appl. Supercond.*, **28**: 1700205 (2018).
26. S. Khan, B. A. Primavera, J. Chiles, A. N. McCaughan, S. M. Buckley, A. N. Tait, A. Lita, J. Biesecker, A. Fox, D. Olaya, R. P. Mirin, S. W. Nam, and J. M. Shainline, *Nat. Electron.*, **5**: 650 (2022).